Hindawi
Advances in Civil Engineering
Volume 2020, Article ID 8893842, 10 pages
https://doi.org/10.1155/2020/8893842

Research Article

The Stability Analysis of Roadway near Faults under Complex High Stress

Biao Zhang,[1] Huaqiang Zhou,[1] Qingliang Chang,[1] Xu Zhao,[2] and Yuantian Sun[1]

[1]*Key Laboratory of Deep Coal Resource Mining, Ministry of Education of China, School of Mines, China University of Mining and Technology, Xuzhou 221116, China*
[2]*School of Civil, Environmental and Mining Engineering, The University of Western Australia, Perth, Australia*

Correspondence should be addressed to Yuantian Sun; yuantiansun@cumt.edu.cn

Received 6 September 2020; Revised 27 October 2020; Accepted 2 November 2020; Published 3 December 2020

Academic Editor: Hualei Zhang

Based on geological conditions of 3318 working face haulage roadway in Xuchang Coal Mine, as well as the space-time relationship with surrounding gob, theoretical analysis and numerical simulation were used to study the influence of fault structure on the original rock stress of 3318 working face transport roadway. Considering the composite action of the leading supporting pressure of 3318 working face and the structure and the lateral supporting pressure of gob, the stress distribution and deformation law of roadway under the complex and high-stress condition are studied. The results show that, under the superposition of lateral abutment pressure of goaf and abutment pressure of adjacent working face and fault structure, the peak stress of roadway roof and floor moves to the surface of roadway surrounding rock, and its distribution law changes from obvious symmetry to asymmetry; surrounding rock on both sides of roadway forms asymmetric circular concentrated stress area; roof and floor and two sides of roadway show asymmetric characteristics. This reveals the stability characteristics of roadway surrounding rock under the action of multiple perturbation stresses.

1. Introduction

The Xuchang Coal Mine has entered into the middle-post stage of life cycle: almost all the mining areas with simple geological conditions have been extracted, while the majority of the remaining mining areas are heavily influenced by geological structures, where the geological conditions of coal seams are complex and many geological structures such as faults are developed. Meanwhile, the current main working face is surrounded by goafs; hence, roadways of working face are always within the strong influence range of the lateral abutment pressure applied from goafs. Under the superimposed influences of the geological structure and the supporting pressure of adjacent working faces, the roadway had been repaired many times even before the mining operation and subjected to effects of secondary high stress caused by multiple disturbances for a long time. Currently, focusing on the fault activation mechanism and main influencing factors caused by mining operations near fault area, various scholars have carried out relevant research and some useful conclusions are obtained [1–3].

Meanwhile, many other scholars have done much research on the distribution mechanism of abutment pressure of surrounding rock during and after the working face mining process [4–7]. After taking the influencing factors of abutment pressure into account, they proposed the analytical and numerical solutions of advance abutment pressures from the working face and lateral abutment pressures from the goaf [5, 8–14]. And then based on elastic-plastic theory, the stability of deep broken roadway under heterogeneous high ground stress is studied by combining analytical method with finite difference numerical method. Based on the principle of equivalent deformation, the mechanical model of segmental shotcrete linings with yielding elements is established using the homogenization approach, Analytical prediction for the behaviour of ductile tunnel linings is provided [15–18]. An investigation on an analytical design method for ductile tunnel linings is performed. And

the foam concrete can absorb a certain amount of rock creep deformation and reduce the characteristics of lining pressure, so as to deal with the large deformation of the squeezed roadway [19–23]. The above research conclusions have laid the foundation stone of accurate acquirement of surrounding rock stability of underground space under the influences of fault and abutment pressure. However, the existing research results are mostly obtained based on single factor, that is, considering either the effect of faults or the influence of faults and single disturbance of abutment pressure, while the multiple superimposed effects of the lateral abutment pressure of the fault and the goaf and the advance bearing pressure of the working face are less involved [24–27].

Focusing on above problems and taking account of actual geometrical conditions of the typical complex high-stress roadway, No. 3318 working face haulageway, this paper analysed the superimposed effects of the geological structure and the lateral abutment pressure of adjacent goaf and considered the combined influences of advance abutment pressures from the working face and lateral abutment pressures from the goaf. Therefore, the stress distribution features and deformation and fracture characteristics of the roadway under complex high-stress conditions were obtained, paving the way for other stability studies of underground structures in complex high-stress fault areas with similar conditions.

2. The Basic Geometrical Conditions of Complex High-Stress Roadway

2.1. The Overview of No. 3318 Working Face Haulageway. Figure 1 shows the layout of the 3318 working face. The 3318 working face is located between the Huangqiao East fault and the Huangqiao fault. The length of the working face changes with the distance between these two faults: the working face length is reduced from 128 m at the time of initial mining to about 40 m at the end of mining. Specifically, the north side of the 3318 working face haulageway is the goaf of 3302 upper working face. The space between these two working faces is about 60 m wide, where the Huangqiao East fault is developed inside.

3318 working face haulageway takes the responsibilities of coal transportation, pipeline laying, equipment installation, ventilation, pedestrians, etc. during the extraction of 3318 working face. The roadway was designed to be about 1030 m and 2 years of service life. The roadway was arranged inside of the 3 lower coal seam and was driven along the coal seam floor. The elevation of the roadway was about +40 m relative to the ground level, and −320 m relative to the underground level, with the maximum depth of the roadway of about 360 m below the surface. The roadway adopted a rectangular section. Specifically, the size of extracted section was 16 m^2, with dimensions of 5000 mm (width) by 3200 m (height); the net area of the roadway section was 14.88 m^2, with dimensions of 4800 mm (width) by 3100 mm (height). The thickness of the coal seam varied between 3.50 and 4.50 m, with an average of 4.00 m. The immediate roof of coal seam was an interbedded layer of mudstone and siltstone and the main roof was mainly siltstone and fine sandstone, while the immediate and main floor were mudstone mixed with sandy mudstone and fine sandstone, respectively.

2.2. Instability Characteristic of 3318 Working Face Haulageway. Under the superposition of fault structure, lateral abutment pressure, and supporting pressure of the working face, significant deformation appeared in 3318 working face transport roadway (as shown in Figure 2). The characteristics of instability were as follows: the roof was completely sunken, accompanied with wrinkle deformation (as shown in Figure 2(a)); two sides strongly converged, while convergence of the side near to the goaf was larger than that of the side near to the working face (as shown in Figures 2(b) and 2(c)), showing a significant asymmetric deformation feature; the roadway had a strong floor lift, with the maximum deformation being more than 800 mm. The cracks that developed on the floor were visible, and floor lift had also some asymmetrical features; that is, the maximum position of the floor deformation was closer to the side of the working surface (as shown in Figure 2(d)).

According to the instability characteristics of the roadway, under the superposition of multiple disturbance stresses, the overall sinking of the roof, strong inside convergence of the two sides and asymmetrical deformation characteristics of the serious floor lift indicated that it was difficult to reach a stable state for the roadway during the service life. Therefore, it was urged to have a thorough study of stability characteristics of the roadway.

3. Stress Distribution Characteristics of Roadway near Fault under Lateral Abutment Pressure

To investigate the stability of surrounding rocks of such stressed roadways, a Flac3D three-dimensional numerical analysis model with dimensions of 300 m (length) by 200 m (width) by 200 m (height) was established (shown in Figure 3). The surrounding sides of the model were set as fixed velocity boundaries, the bottom boundary was the fixed displacement boundary condition, and the top was the stress boundary condition applied with uniform load of 6.5 MPa, simulating the weight of the overlying rock layer with 260 m thickness. The 3318 working face and its mining roadways were located in the middle part of the model, where the horizontal distance between the transport roadway and the fault was 20 m, and the horizontal distance from the edge of the adjacent goaf was 60 m. At the same time, the adjacent working face is modelled by semi-infinite mining method; that is, the adjacent goaf is located at the left boundary of the model. The mesh stress and deformation iterations in the model used the Mohr–Coulomb strength criterion. The fault was simulated by the interface command with the sliding mode turned on. According to the field geological data and the test results of physical and mechanical property indexes of rock core, and according to the RMR system classification of engineering rock mass, the calculation parameters of this

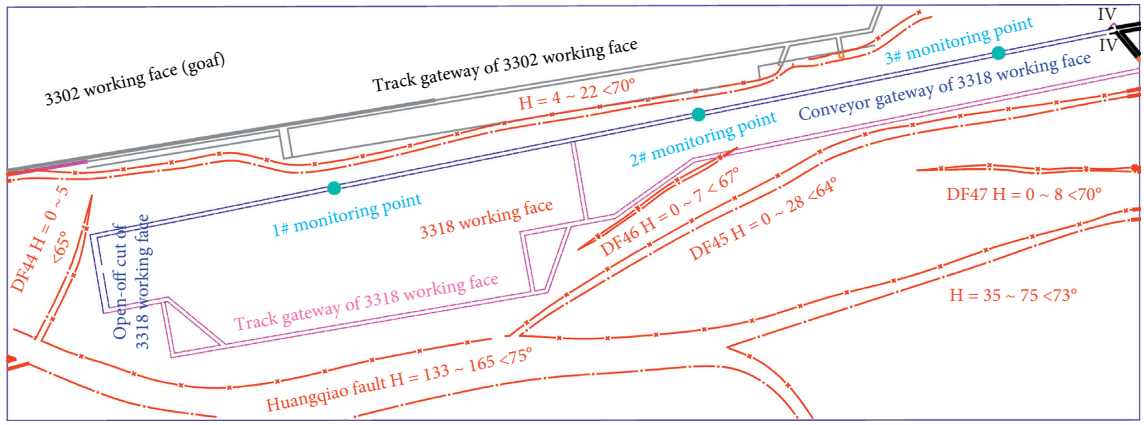

Figure 1: The layout of haulageway of 3318 working face.

Figure 2: Instability characteristics of haulageway.

numerical analysis are reduced according to the relevant formula. Table 1 shows the calculation parameters of surrounding rock mechanics after weakening according to the classification of engineering rock mass.

3.1. Stress Distribution Law of Rock Mass near the Fault Area. To the 3318 working face transportation roadway of Xuchang Coal Mine, it was strongly influenced by the normal fault nearby and showing the stress distribution characteristics of the normal fault zone; that is, the rock mass stress near the fault decreased slightly, and the phenomenon of stress discontinuity occurred at the fault contact surface, as shown in Figure 4. Along the contact surface between hanging wall and footwall, the maximum difference of principal stresses in the same horizontal plane reached 0.5 MPa, and concentration of stress appeared at the floor of hanging wall of the fault, while the stress decreased at the bottom of the footwall, showing the influence regulations of the normal fault on the stress of the rock stratum near the roadway.

3.2. Stress Distribution Laws of Near-Fault Roadway under the Influence of Lateral Abutment Pressure. After the structure of fault and the lateral abutment pressure exerted by adjacent working face became gradually stable, the roadway was excavated in the numerical model and the stress distribution

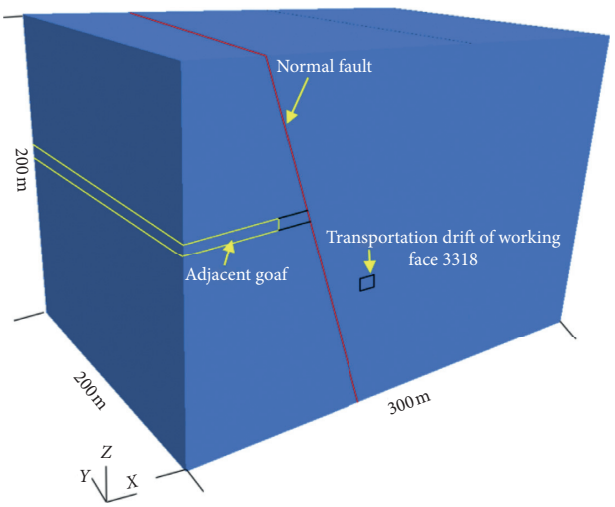

Figure 3: The numerical model for analysis.

Table 1: Each layer of rock physical and mechanical parameters in model.

Rock stratum	Density (kg/m^3)	Tension (MPa)	Friction (°)	Cohesion (MPa)	Bulk (GPa)	Shear (GPa)
Sandstone	2600	40	42	1.60	8.4	3.00
Siltstone	2400	5.6	30	1.50	1.9	0.90
Coal	1380	1.9	28	0.12	0.9	0.09
Sandy mudstone	2400	6.0	35	1.20	1.9	0.80
Sandstone	2600	35	45	1.60	8.8	6.20

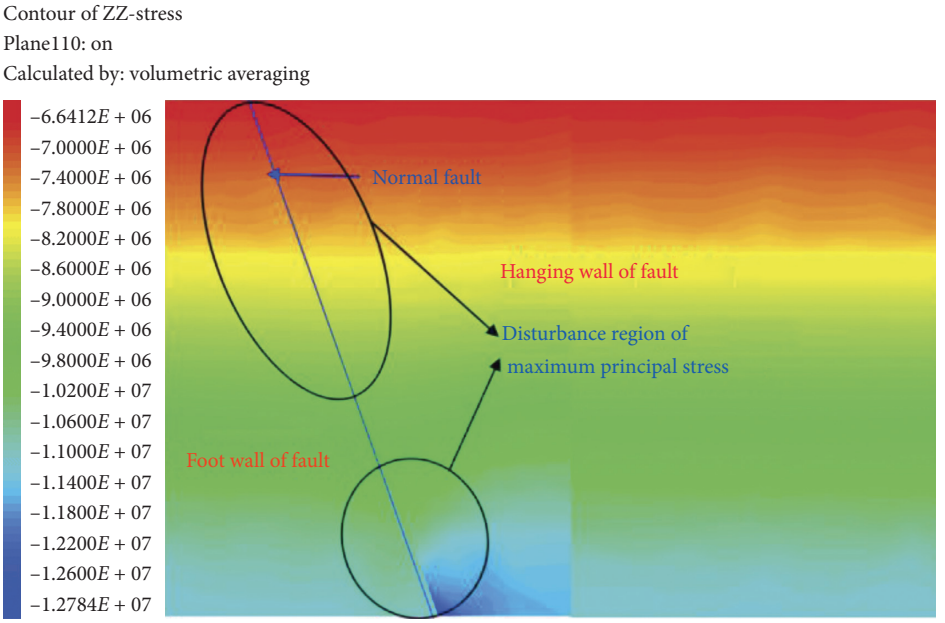

Figure 4: Vertical stress distribution law of rock mass near the fault area.

law of surrounding rock is shown in Figure 5. The vertical stresses of the floor and roof rock layers of the roadway were significantly reduced, wherein the stress reduction range of roof was about 2.4 m and that of floor was about 2.6 m. Vertical stress concentration occurred in both sides of the roadway. The peak stress concentration of the left side was 4 m away from the surrounding rock surface of the roadway, with peak value being 14.9 MPa. It should be noted that this concentrated stress disturbance region and the concentrated stress area of the fault zone were connected. Because the concentrated stress near the fault was mainly influenced by the lateral abutment pressure of the goaf adjacent to the 3302 working face, the left side of 3318 working face haulageway was strongly influenced by the abutment pressure of

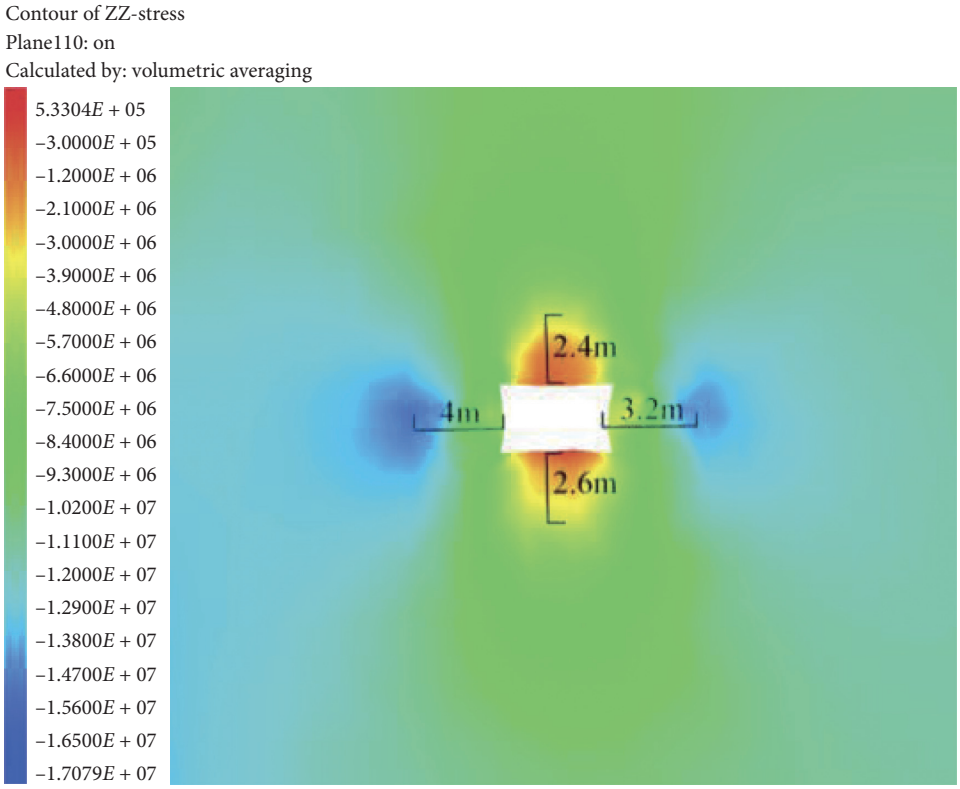

Figure 5: The vertical stress distribution of surrounding rock in the haulageway of No. 3318 working face.

protective coal pillars, which promoted the stress concentration factor to be 1.7. In addition, the vertical stress peak of the right side of the roadway was 3.2 m away from the surrounding rock surface of the roadway, with the peak value of concentration stress and concentration factor being 14.6 MPa and 1.66, respectively. The concentrated stress distribution range of the right surrounding rock was also smaller than that of the left side.

Compared to the stress distribution in surrounding rock of the air-return roadway of the 3318 working face which was not affected by the fault structure and the lateral abutment pressure (shown in Figure 6), under the influence of the stress superposition, the stress reduction range of the roof of 3318 working face haulageway was reduced by about 1 m, while the distance between the concentrated stress peaks of the two sides and the surface of the roadway was reduced by 0.2–0.6 m. At the same time, the peak stress concentration of the surrounding rock of both sides increased by about 11 MPa. It was shown that the lateral abutment pressure of the adjacent goaf had an influence range of more than 80 m. Although there was a tensile normal fault and discontinuity of stress near the fault, the high abutment pressure still significantly increased the surrounding rock stress of the 3318 working face, shifted the peak points of concentrated stress to the surrounding rock surface of the roadway, and caused strong deformation of the jointed rock mass on the surface of the transport roadway. In addition, the stress distribution law of the surrounding rock of the roadway showed a gradual evolution from significant symmetry to asymmetry; that is, left-sided surrounding rock near the fault was subjected to higher concentrated stress, and the concentrated stress disturbance range was larger. The above analysis well explained the reason for the asymmetric deformation characteristics of the 3318 working face haulageway from the perspective of stress distribution.

4. Stability Characteristics of Surrounding Rock in Complex High-Stress Roadway

4.1. Stress Distribution Law of Surrounding Rock in Complex High-Stress Roadway. Figure 7 shows the vertical stress distribution of surrounding rock in complex high-stress roadway. During the mining process of the 3318 working face, the roof rock layer gradually bended and sank, and the overburden rock load shifted to the surrounding rock of the roadway, forming a semicircular concentrated stress zone in the surrounding rock in the roadway and showing asymmetric characteristics.

According to the figure, the peak concentration of the surrounding rock of the right side of the roadway reached 22.1 MPa with the stress concentration factor being about 2.5, and the peak position was 5.5 m away from the surrounding rock surface of the right side; on the left side, the stress concentration was slightly smaller. However, the peak concentration of concentrated stress still reached about 21 MPa, located at 4.5 m away from the surface of the surrounding rock. In addition, the surrounding rock stress reduction areas in the floor and roof of the roadway were both large (4 m and 3.8 m, respectively), and the stresses dropped significantly in the range of 0–3 m in floor and roof, lower than 2 MPa.

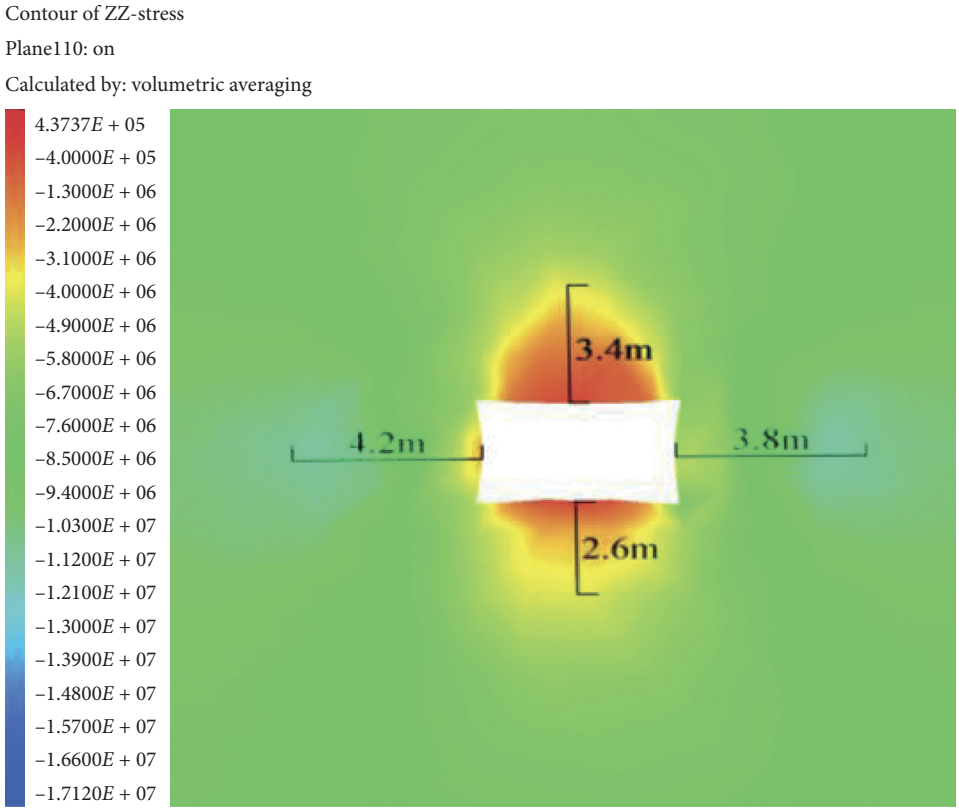

Figure 6: The vertical stress distribution of surrounding rock in the air-return roadway of No. 3318 working face.

Compared with stress state of surrounding rock of the 3318 working face before the mining operations (shown in Figure 5), the concentrated stress range of the two sides had significantly developed, especially for surrounding rock on the right side. The peak of concentrated stress increased sharply from 14.6 MPa to more than 22 MPa. And the concentrated stress strongly affected the area from a circular area with a radius of about 3 m to a semicircular area with a radius of about 20 m (approximate arc-shaped distribution in the illustrated section), resulting in right-wall surrounding rock being strongly influenced by the superposition of lateral support pressure and presupporting pressure, which accelerated the instability of rock mass after the peak pressure; at the same time, the peak of concentrated stress of left-side surrounding rock also increased significantly from 14.9 MPa to about 21 MPa, and the concentrated area and stress peak influencing area expanded from a circular area with a diameter of about 4 m to a semicircular area with a diameter of about 18 m, and the range of high concentrated stress was also rapidly expanded.

4.2. Deformation Law of Surrounding Rock in Complex High-Stress Roadway. Figure 8 shows the deformation law of the surrounding rock of two sides. The deformation in X-direction of different parts of two sides was different: deformation of lower part was larger than those of middle area and upper area, being 520 mm, 270 mm, and about 100 mm, respectively; in the stabilization process of surrounding rock, the lower-middle part was significantly affected by the displacement of the surrounding rock of the goaf; that is, during the steps from 3300 to 6000, the deformation of the surrounding rock of lower and middle increased from 320 mm and 200 mm to 520 mm and 270 mm, respectively. Within the range of 0–2 m near the surface of the surrounding rock, deformations of lower-middle-upper three parts of two sides were all significantly reduced. The maximum change occurred in the lower part, followed by the middle and the top areas; in the range of 2–4 m, the surrounding rock of the two sides had a small deformation, less than 70 mm. The deformation beyond 4 m was relatively small and finally stabilized at around 10 mm. Therefore, the strong influencing zone of the surrounding rock of two sides is in the range of 0–2 m, while the deformation of the surrounding rock in the range of 2–4 m is relatively small.

Figure 9 shows the deformation laws of surrounding rock of roadway roof at different areas. During the stability process of surrounding rock in the 3318 working face transportation roadway, the deformation process of the surrounding rock in the z-direction was similar to that of the left side. In step 3300-6000, the deformation of the surrounding rock increased sharply. At the same time, the deformation of the surrounding rock of the roof presented weak symmetrical distribution along the midline, wherein the deformation at the intersections of roof and two sides was relatively small and the deformation trends are similar; both increased from the initial 220 mm to 530–540 mm. The deformations of three positions in the roof were uniform and relatively large, increasing from initial 220 mm to 650 mm or even more.

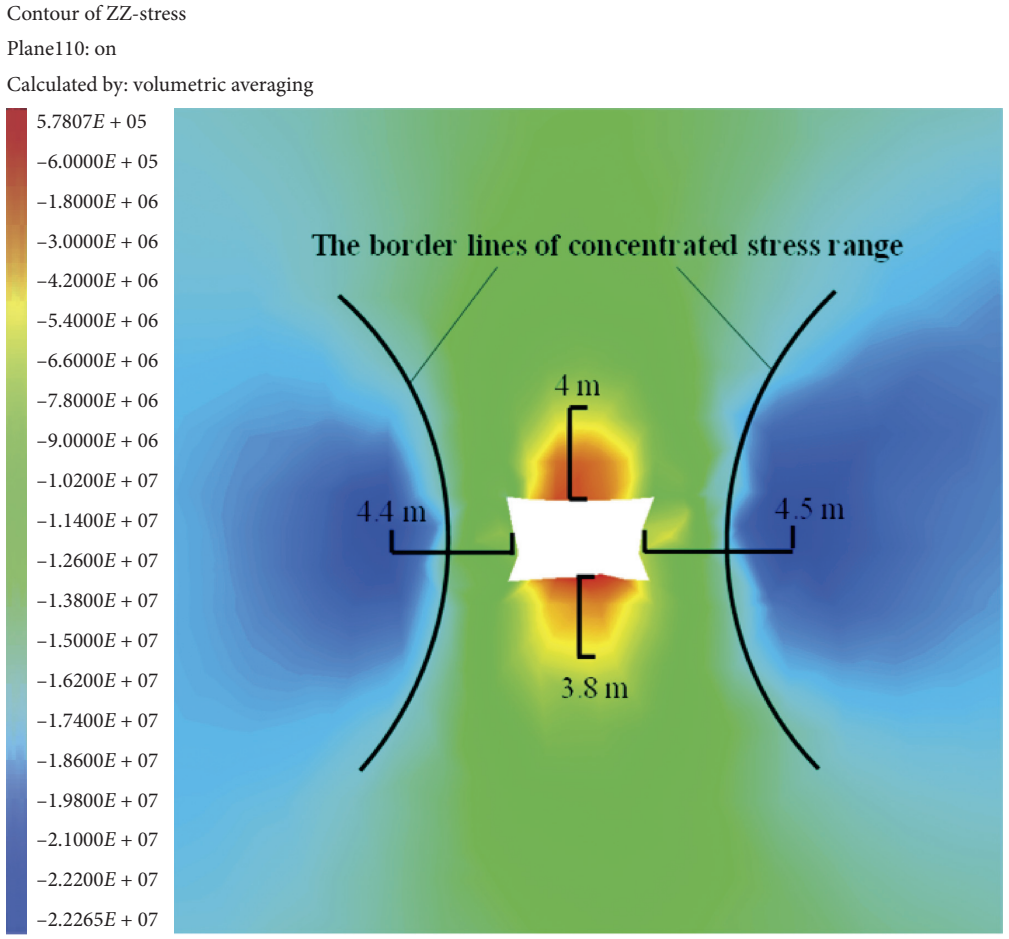

Figure 7: The vertical stress distribution of surrounding rock in complex high-stress roadway.

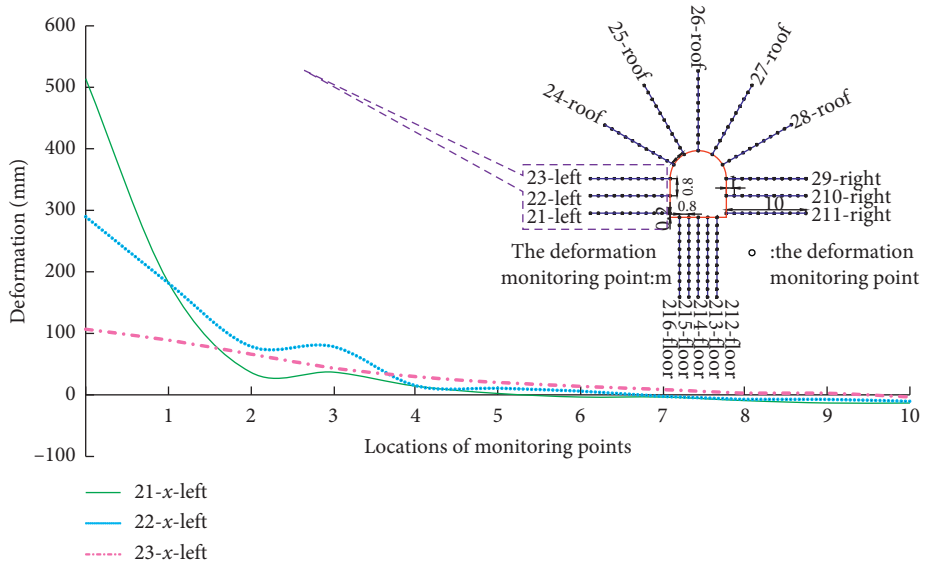

Figure 8: The deformation law of the surrounding rock of roadway sides.

With the increase of the distance from the surface of roof, the deformation of the surrounding rock fluctuated significantly, and the deformation of the surrounding rock changed sharply in the range of 0–2 m. The trend of the surrounding rock deformation was consistent at the three locations of the roof and the deformation at the 2 m position

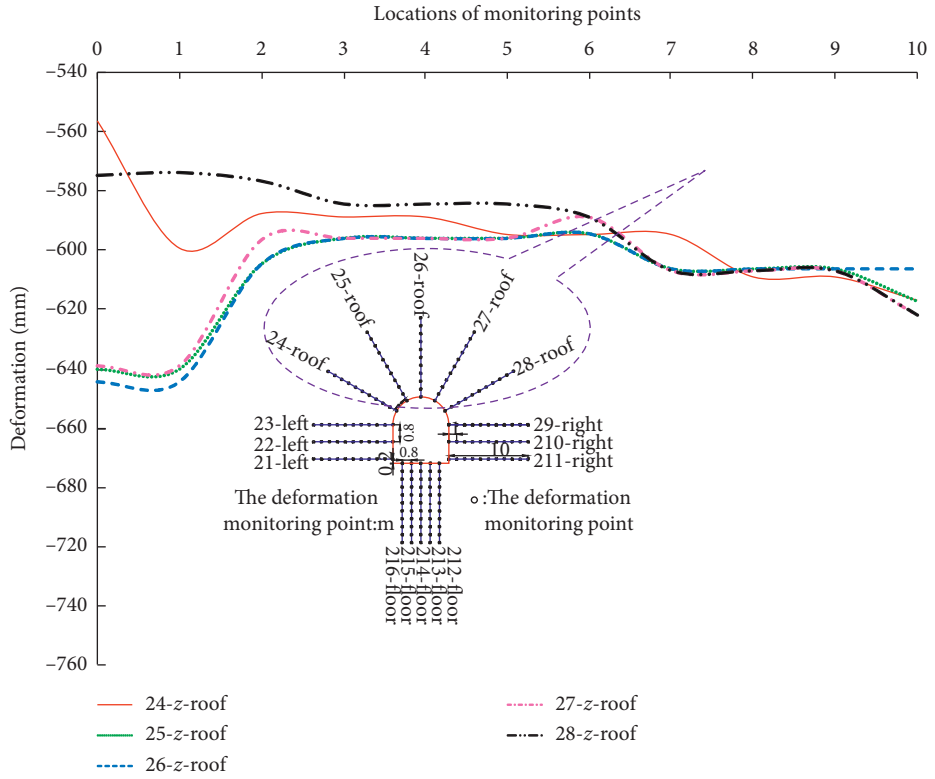

Figure 9: The deformation law of the surrounding rock of roadway roof.

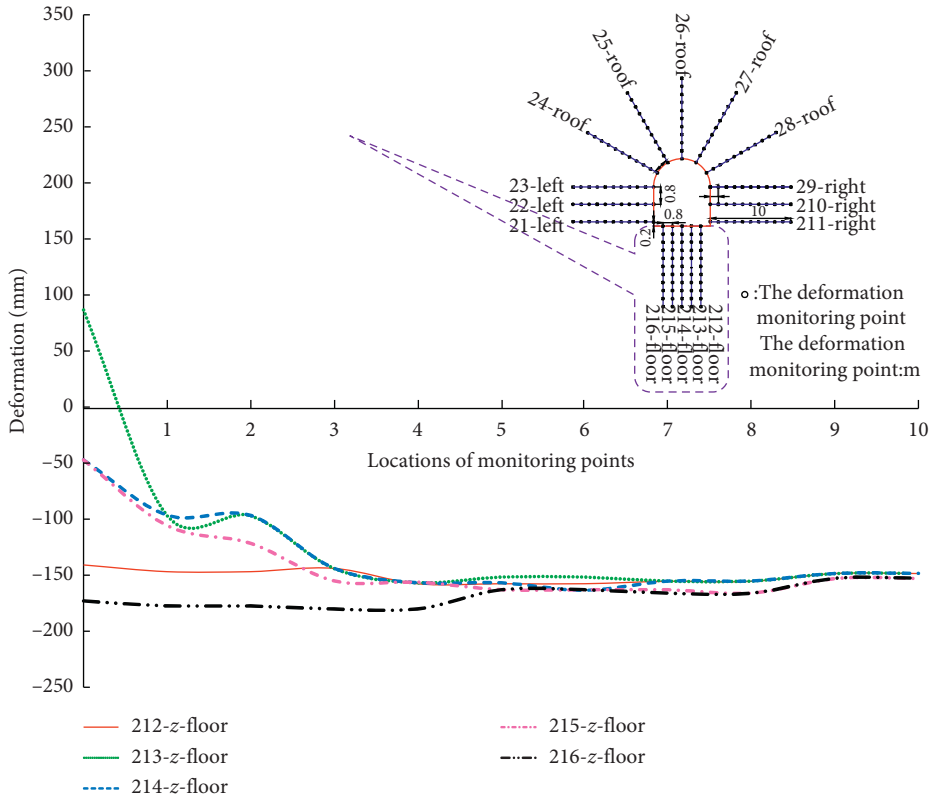

Figure 10: The Z-direction deformation law of the surrounding rock of roadway floor.

was reduced to about 600 mm, indicating that the roof strata in the range of 0–2 m occurred a 40–50 mm separation; the deformation of the roof rock mass in the range of 2–6 m was consistent, indicating little separation has occurred; the surrounding rock within the range of 6–10 m was influenced by the sinking of the main roof strata, resulting in a slight increase of deformation.

According to Figure 10, the deformation at the intersections of roof and two sides was relatively large, about 140 mm and 170 mm, respectively. The deformation of the middle-lower part of the left side was relatively small, only about 48 mm, while that of the right side reached 80 mm. In addition, with the increase of the distance from the surface of the floor, there was no significant change at the intersections of roof and two sides, while the other parts changed sharply in the range of 0–4 m, wherein at depth of 0.5 m, the surrounding rock on the right side of the floor showed the points with zero displacement. It was therefore shown that, in the 0–4 m range, the floor stratum had significant tensile and shear failure characteristics and significant asymmetric deformation trend along the midline.

The analysis of the stress distribution laws of the surrounding rock of the roadway showed that the floor strata of the roadway were affected by the triangular block rotation movement from the goaf side of 3318 working face. The deformation of the surrounding rock of the floor was significantly increased by more than 100 mm, especially at middle-left, middle, and middle-right locations of the floor where variation and deformation of surrounding rock were strongly influenced. Before the influence of the advance abutment pressure of the 3318 working face, zero deformation points in surrounding rock existed in the middle and middle-left areas of the floor. However, after being subjected to the influence of the advance abutment pressure, the above two areas deformed to the direction of goaf.

5. Conclusion and Prospect

Under the superimposed influences of the lateral abutment pressure of goaf and abutment pressure of adjacent working faces and fault structure, the surrounding rock of roadway shows the following characteristics:

(1) The vertical stress of the floor and roof of the roadway was significantly reduced and the stress concentration areas of the two sides and fault area were penetrated. Furthermore, the stress peak shifted to the surrounding rock surface of the roadway and the stress distribution law changed from significant symmetry to asymmetrical feature.

(2) The stress field in surrounding rock of the roadway was strongly influenced by the bending and sinking of the roof strata, the overburden load was transferred to the surrounding rock of the roadway, and an asymmetric circular concentrated stress zone was formed in the surrounding rock of the two sides.

(3) The roof, floor, and both sides of the roadway are characterized by sudden increase, violent fluctuation, and strong asymmetry. At the same time, influence of the advance abutment pressure on deformation in different parts of roadway was significantly different.

The deformation of roadway surrounding rock may be significantly different due to the different nature of fault and the lateral abutment pressure of goaf. Due to the length of an article, this paper has not carried out the research on the movement and deformation law of roadway surrounding rock under the influence of reverse fault. Therefore, in the future, the stability of surrounding rock of complex high-stress roadway under the influence of reverse fault will be further studied.

Data Availability

The Microsoft Excel Worksheet data used to support the findings of this study are available from the corresponding author (yuantiansun@cumt.edu.cn) upon request.

Conflicts of Interest

The authors declare no conflicts of interest.

Acknowledgments

This study was financially supported by the Fundamental Research Funds for the Central Universities (grant number: 2020ZDPY0221) and the "National Key Research and Development Program (grant number: 2016YFC0600901)."

References

[1] L. Wang, W.-J. Wang, and J. Huang, "Numerical analysis of the effect of advanced abutment pressure on fault actication," *Mining Technology*, vol. 11, no. 3, pp. 50–52, 2011.

[2] W. Jiu-chuang, G. Min, and Z. Li, "Influence of fault dip angle of coal face abutment pressure numerical simulation research," *Coal Technology*, vol. 33, no. 6, pp. 135–137, 2014.

[3] H. Basarir, Y. Sun, and G. Li, "Gateway stability analysis by global-local modeling approach," *International Journal of Rock Mechanics and Mining Sciences*, vol. 113, pp. 31–40, 2019.

[4] H.-R. Liu, Z.-C. Li, J. Dai, and H. Tian, "Abutment pressure distribution and impact analysis on the plate in normal faults," *Journal of Shandong University of Science and Technology (Natural Science)*, vol. 33, no. 3, pp. 48–53, 2014.

[5] Y. Sun, G. Li, J. Zhang, and D. Qian, "Experimental and numerical investigation on a novel support system for controlling roadway deformation in underground coal mines," *Energy Science & Engineering*, vol. 8, no. 2, pp. 490–500, 2020.

[6] M. Qing-Xin, W. Yang-bao, L. Wei-xin, and S. Li-thong, "Study on law of abutment stress distribution in lateral coal body near face goaf," *Coal Technology*, vol. 37, no. 5, pp. 72–75, 2018.

[7] W. Shi-ming and W. Yang, "Analysis of research status on distribution characteristic of abutment pressure in surrounding rock," *Coal Science and Technology*, vol. 46, no. S1, pp. 18–22, 2018.

[8] L. V. Jian-wei and D. Jin, "Influence analysis of overlying strata on bearing pressure of working face," *Journal of China Coal Society*, vol. 44, no. 11, pp. 72–77, 2018.

[9] Y. Sun, G. Li, N. Zhang, Q. Chang, J. Xu, and J. Zhang, "Development of ensemble learning models to evaluate the strength of coal-grout materials," *International Journal of Mining Science and Technology*, 2020.

[10] P. Xiao, S. G. Li, H. Lin, P. Zhao et al., "Distribution characteristics of stope support pressure for different main Key layer position," *Safety in Coal Mines*, vol. 45, no. 12, pp. 211–213, 2014.

[11] J.-W. Zhang, Y-D Gu, and J.-A. Wang, "Research on support pressure distribution characteristics of steeply inclined coal seam," *Safety in Coal Mines*, vol. 46, no. 5, pp. 67–70, 2015.

[12] Z.-G Wu, "Study on calculation formula of abutment pressure peak value of face," *Coal Technology*, vol. 34, no. 12, pp. 25-26, 2015.

[13] Y. Sun, G. Li, H. Basarir et al., "Laboratory evaluation of shear strength properties for cement-based grouted coal mass," *Arabian Journal of Geosciences*, vol. 12, no. 22, p. 690, 2019.

[14] X.-S Wang, "Study on influencing range of support pressure in working face," *Coal Science and Technology*, vol. 41, no. S2, pp. 97–99, 2013.

[15] J.-J Jiang, L. Xiao-lu, and O. Zeng-Hua, "Numerical simulation research on abutment pressure distribution in extra-thick coal seam fully-mechanized caving stope," *Safety in Coal Mines*, vol. 47, no. 1, pp. 208–211, 2016.

[16] Y. Sun, J. Zhang, G. Li et al., "Determination of young's modulus of jet grouted coalcretes using an intelligent model," *Engineering Geology*, vol. 252, pp. 43–53, 2019.

[17] Q.-H Ren and X.-Y Zhang, "Numerical simulation analysis of slope length effect on evolution of abutment pressure in deep stope," *Safety in Coal Mines*, vol. 48, no. 9, pp. 201–203, 2017.

[18] X.-J. Liu, Q. Wang, and D. Jin, "Study on horizontal pillars abutment pressure propagation laws in floor," *Safety in Coal Mines*, vol. 44, no. 12, pp. 58–61, 2013.

[19] Y. Sun, J. Zhang, G. Li, Y. Wang, J. Sun, and C. Jiang, "Optimized neural network using beetle antennae search for predicting the unconfined compressive strength of jet grouting coalcretes," *International Journal for Numerical and Analytical Methods in Geomechanics*, vol. 43, no. 4, pp. 801–813, 2019.

[20] J. Zhu-Peng, T. Qin, and J.-W. Zhang, "Analysis of abutment pressure distribution characteristics and influencing factors of deep mining height face," *Coal Science and Technology*, vol. 46, no. S1, pp. 97–99, 2018.

[21] Y. Sun, G. Li, J. Zhang, and J. Xu, "Failure mechanisms of rheological coal roadway," *Sustainability*, vol. 12, no. 7, p. 2885, 2020.

[22] Y. Huang, A. Zhao, T. Zhang, and W. Guo, "Plastic failure zone characteristics and stability control technology of roadway in the fault area under non-uniformly high geostress: a case study from yuandian coal mine in Northern Anhui Province, China," *Open Geosciences*, vol. 12, no. 1, 2020.

[23] Y. Sun, G. Li, J. Zhang, and D. Qian, "Stability control for the rheological roadway by a novel high-efficiency jet grouting technique in deep underground coal mines," *Sustainability*, vol. 11, no. 22, p. 6494, 2019.

[24] K. Wu, Z. Shao, and Q. Su, "An analytical design method for ductile support structures in squeezing tunnels," *Archives of Civil and Mechanical Engineering*, vol. 20, no. 3, p. 91, 2020.

[25] Y. Sun, G. Li, and J. Zhang, "Investigation on jet grouting support strategy for controlling time-dependent deformation in the roadway," *Energy Science & Engineering*, vol. 8, no. 4, pp. 1–8, 2020.

[26] K. Wu and Z. Shao, "Visco-elastic analysis on the effect of flexible layer on mechanical behavior of tunnels," *International Journal of Applied Mechanics*, vol. 11, no. 3, 2020.

[27] K. Wu, Z. Shao, and S. Qin, "A solution for squeezing deformation control in tunnels using foamed concrete: a review," *Construction and Building MaterialsVolume*, vol. 257, Article ID 119539, 2020.